RSC Advances

PAPER

View Article Online
View Journal | View Issue

Cite this: *RSC Adv.*, 2021, **11**, 21137

An ultrasensitive colorimetric and fluorescence dual-readout assay for glutathione with a carbon dot–MnO_2 nanosheet platform based on the inner filter effect†

Mengyuan He, * Ning Shang, Bo Zheng and Gege Yue

An ultrasensitive colorimetric and fluorescence dual-readout assay based on the inner filter effect (IFE) was developed for glutathione (GSH) determination, in which carbon dots (C-dots) were used as a fluorophore and MnO_2 nanosheets as an absorber. Due to the excellent optical absorption properties of MnO_2 nanosheets and the good spectral overlap between the fluorophore and absorber, MnO_2 nanosheets could effectively quench the fluorescence of C-dots *via* the IFE. As the target, GSH could reduce MnO_2 nanosheets to Mn^{2+} ions, which inhibited the IFE and resulted in the fading of solution color and the recovery of the fluorescence signal. And these two kinds of signals were respectively used for qualitative and quantitative detection of GSH. The results showed that this proposed assay could distinguish 10 μM GSH with the naked eye and quantitatively detect GSH within the concentration range of 0.1–400 μM. The limit of detection was 6.6 nM. Moreover, this assay showed sensitive responses in human serum and urine samples, which indicated that this IFE-based assay has great potential in GSH-related clinical and bioanalytical applications.

Received 26th March 2021
Accepted 2nd June 2021

DOI: 10.1039/d1ra02411f

rsc.li/rsc-advances

Introduction

Glutathione (GSH), a biological molecule containing a mercaptan group, plays important roles in biological systems, such as maintaining the processes of intracellular redox activity, intracellular signal transduction, apoptosis and proliferation, by participating in reversible redox homeostasis processes.[1,2] Aberrant levels of GSH are closely related to many diseases, such as cancer, immune system disease, liver injury, and Parkinson's disease.[3] Therefore, the sensitive and selective detection of GSH has been of great importance to scientific researchers. There are many methods that have been developed for GSH detection, including electrochemical,[4] electrochemiluminescence,[5] photoelectrochemistry,[6] mass spectrometry,[7] enzyme-linked immunosorbent assay (ELISA),[8] surface-enhanced Raman scattering (SERS),[9] fluorescence spectroscopy[10] *etc.* In these methods, fluorescence analysis is simple, sensitive and non-destructive, so it has been widely considered by researchers. Organic dyes and fluorescent nanomaterials including quantum dots (QDs),[11,12] upconversion nanoparticles (UCNPs),[13] persistent luminescence nanoparticles,[14] graphitic-C_3N_4,[15] metal nanoparticles[16–18] and so on have been used for GSH detection.

Carbon dots (C-dots), with many excellent properties, such as easy preparation, tunable excitation and emission spectra, high photostability, low toxicity, and excellent biocompatibility, have shown good application value in the fields of biosensing and bioimaging.[19,20] Compared to other fluorescent nanoparticles such as QDs and UCNPs, C-dots have more accessible raw materials, simple preparation method, and low intrinsic toxicity.[21–24] Because of these unique properties, carbon dots have attracted more and more attention as fluorescent probes and been used to detect many biological molecules, *e.g.* ascorbic acid (AA),[25] uric acid,[26] dopamine[27] and so on.

As a class of two-dimensional transition metal dioxides, manganese dioxide (MnO_2) nanosheets, have been applied in many fields including energy generation, photocatalysis, sensing, and photothermal therapy, due to its outstanding properties including large specific surface area, fast electron transfer rate, and strong light absorption capability with wide wavelength range.[28–30] In recent years, MnO_2 nanosheets have been used as fluorescence quenchers to constructed bio-/chemical sensing platforms on the basis of fluorescence resonance energy transfer (FRET).[31]

C-dots and MnO_2 nanosheets have been reported as assay platform through the formation of C-dots-MnO_2 nanocomposites, in which MnO_2 nanosheets can be transformed to Mn^{2+} by reductive molecules through the redox reaction.[32–34]

College of Chemistry and Chemical Engineering, Xinyang Normal University, Xinyang 464000, China. E-mail: myhe@xynu.edu.cn

† Electronic supplementary information (ESI) available: Optimization of reaction time, TEM image of the mixture of C-dots–MnO_2 and GSH, the detection results in human urine and so on. See DOI: 10.1039/d1ra02411f

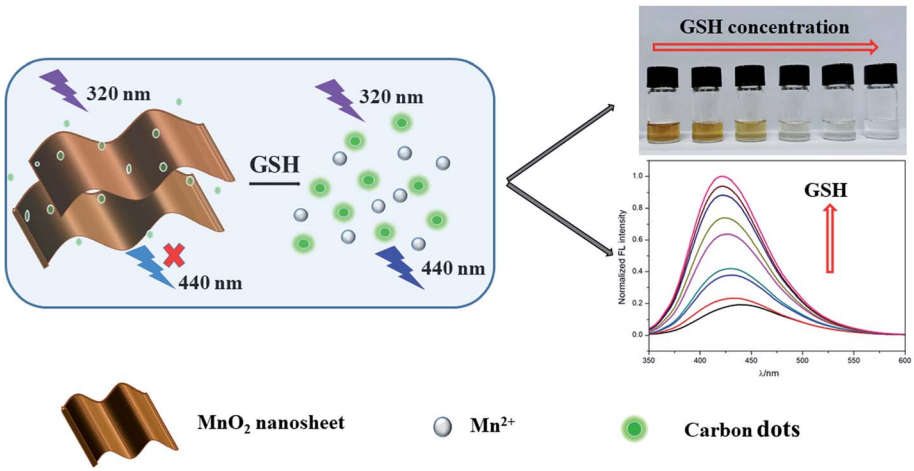

Scheme 1 Schematic illustration of the colorimetric and fluorescence dual-readout assay for GSH based on carbon dots–MnO_2 nanosheets platform.

Most of these were built based on FRET, in which the distance between energy donor and energy acceptor was usually limited to 10 nm. Recently, Tan *et al.* developed a selective and sensitive strategy for dopamine detection based on inner filter effect (IFE), in which C-dots and MnO_2 nanosheets were used as fluorophore and absorber respectively.[35] Compared to FRET, there are no strict requirement for the distance between fluorophore and absorber in IFE and the modification of probes is probably needless.[36–38] However, this assay only use fluorescence signals for detection, and still need the help of analytical instruments.

In this work, an ultrasensitive colorimetric and fluorescence dual-readout assay using C-dots and MnO_2 nanosheets was developed based on IFE for GSH detection in human serum and urine. Citric acid and 6-aminohexanoic acid were used as starting materials to produce C-dots through hydrothermal method. MnO_2 nanosheets were synthesised through the reduction of $KMnO_4$, in which 2-(*N*-morpholino) ethanesulfonic acid (MES) was used as reducing agent. As shown in Scheme 1, owing to the good spectral overlap between the absorption band of MnO_2 nanosheets and the excitation and emission band of the C-dots, MnO_2 nanosheets can effectively quench the fluorescence of C-dots through IFE. When GSH was added, MnO_2 nanosheets were transformed to Mn^{2+} through redox reaction, leading to the elimination of IFE. Thus the color of the solution changed from brown to colorless, which was used for qualitative detection of GSH with naked eye. Simultaneously, the fluorescence of C-dots were recovered, which was used for quantitative detection. Compared with single fluorescence detection mode, this work can achieve qualitative and quantitative detection at the same time without additional equipments, which show great potential in the field of home self-inspection and on-site rapid detection.

Materials and methods

Materials

Glutathione (GSH), citric acid, 2-(*N*-morpholino)ethanesulfonic acid (MES) and different kinds of amino acids were purchased from Sinopharm Chemical Reagent Co., Ltd (Shanghai, China). Dialysis membrane (MWCO = 1000) were from Spectrumlabs (America). Human serum samples were provided by healthy volunteer from Hospital of Xinyang Normal University. Human urine samples were provided by healthy volunteer in our research group.

Apparatus

The morphology of C-dots, MnO_2 nanosheets and C-dots–MnO_2 mixture were characterized by Tecnai G2 F 20 Transmission electron microscope (FEI, America). The zeta potential of carbon dots were measured by Zetasizer Nano ZS laser particle size analyzer (Malvern, England). The XPS spectra were obtained by K-Alpha X-ray electron spectrometer (Thermo Scientific, America). The fluorescence spectra of C-dots were measured by Hitachi F7000 spectrophotometer (Hitachi, Japan). The UV-Vis absorption spectrum of MnO_2 nanosheets was measured by 3900H spectrophotometer (Hitachi, Japan). The luminescence lifetime of C-dots and kinetic experiment was measured with FLS1000 photoluminescence spectrometer (Edinburgh Instruments, UK).

Synthesis of C-dots

1.05 g of citric acid, 0.65 g of 6-aminohexanoic acid and 0.2 g of NaOH were put in 25 mL Teflon autoclave and dissolved by 15 mL water. After reacting at 200 °C for 8 h, the as-obtained brown solution was dialyzed against ultrapure water for three days. The as-prepared C-dots were dried and redispersed in ultrapure water with a final concentration of 4.18 mg mL^{-1}.

Preparation of C-dots–MnO_2 nanosheets mixture

50 μL of C-dots (4.18 mg mL^{-1}) and 30 μL of $KMnO_4$ solution (60 mM) were added into 520 μL MES buffer (10 mM, pH 6.0) successively. After been sonicated for 30 min, a brown C-dots–MnO_2 nanosheets mixture dispersion was obtained. Bare MnO_2 nanosheets were synthesized in the same way in a solution without carbon dots.

GSH detection in aqueous solution

To select optimum concentration of MnO_2 nanosheet, different amounts of $KMnO_4$ solution (60 mM) were first added to C-dots solution and sonicated for 30 min, followed by the fluorescence measurements. For GSH detection, C-dots–MnO_2 mixture was first prepared at the optimized condition. Then different amounts of GSH were added and reacted at room temperature for 20 min. The fluorescence spectra of the mixtures were subsequently measured. To verify the selectivity of this sensors, a serious of distractors were added into C-dots–MnO_2 mixture to replace GSH under the same experimental conditions.

GSH detection in actual samples

C-dots–MnO_2 mixture were then used for GSH detection in human serum and urine samples. Serum samples were diluted with water for 400 times. After been filtered with a 0.22 μm membrane, the urine samples were then centrifuged at 1500 rpm for 5 min to remove urinary sediment. The supernatant were then diluted with water for 400 times. The actual samples were then used as analysis medium, and the same assay procedure as in the buffer was followed.

Result and discussion

Characterization of C-dots and MnO_2 nanosheets

To ensure the analysis performance of our strategy, the as-prepared C-dots was characterized through TEM, UV-Vis absorption spectra, fluorescence spectra, and XPS. The TEM image of C-dots was shown in Fig. 1a, the C-dots are nearly spherical and have good dispersion in water with a narrow diameter range of 4.1 ± 0.7 nm. The lattice fringes of C-dots were shown in Fig. 1b. XPS analysis was used to indentify the surface composition of C-dots. As depicted in Fig. S1a,† the three peaks at 285.3, 399.3, 531.4 eV in full range XPS analysis were associated with C 1s, N 1s and O 1s, which suggests that the C-dots are composed of carbon, nitrogen and oxygen. The C 1s spectrum (Fig. S1b†) could be resolved into five components at 284.1, 284.6, 285.4, 285.8 and 287.7 eV, respectively, which were accordance with sp^2 C–C, C=C, C–N/C–O, C=N, and C=O groups. The UV-Vis absorption spectrum and fluorescence spectra were used to explore the optical properties of C-dots. As shown in Fig. 1c, the typical absorption peak of C-dots was located at 330 nm. The maximum excitation wavelength was located at 320 nm. Under the excitation at this wavelength, C-dots exhibited strong blue emission at 440 nm. What is particularly important is that as-synthesized C-dots shows excellent photostability. As can be seen from Fig. 1d, the fluorescence intensity did not change significantly under continuous irradiation for 1 hour, which guaranteed the superior detection performance of this sensing system.

MnO_2 nanosheets were prepared through the reduction of $KMnO_4$ with MES in ultrapure water. MnO_2 nanosheets showed lamellar structure and good dispersion in aqueous solution (Fig. S2a†). As shown in Fig. S2b,† MnO_2 nanosheets displays

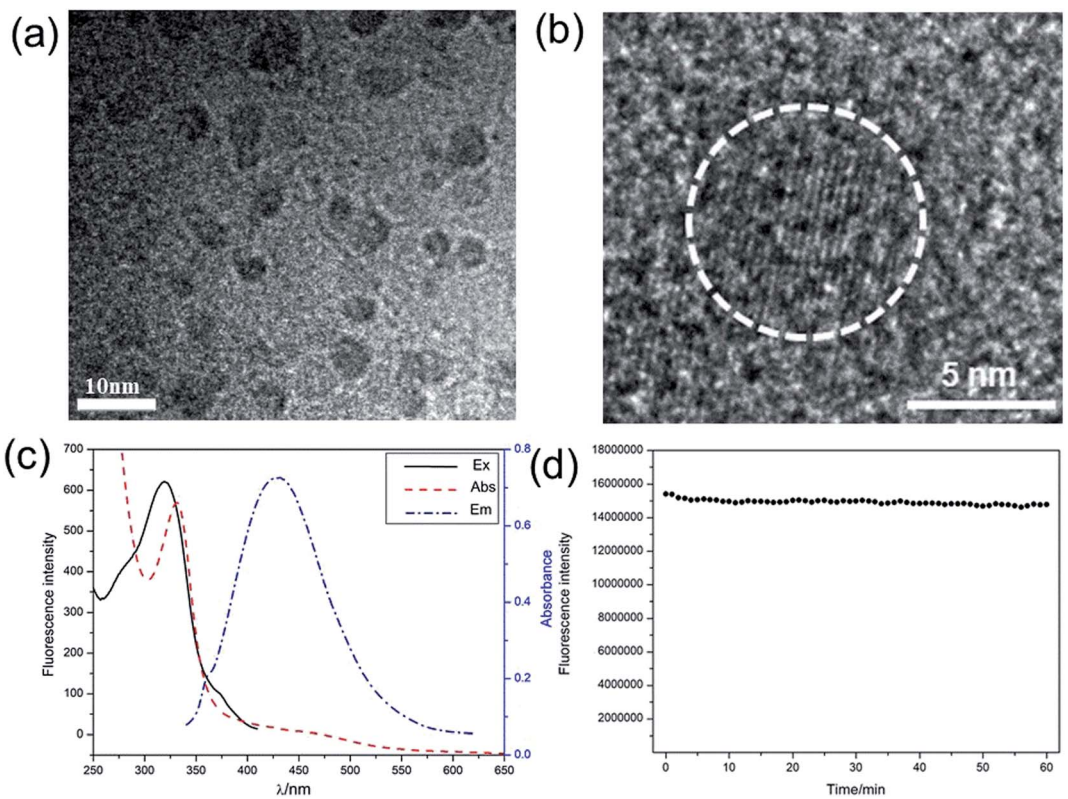

Fig. 1 (a) TEM image of C-dots. (b) HRTEM image of C-dots. (c) The UV-Vis absorption spectrum and fluorescence excitation/emission spectra of C-dots. (d) The photostability of C-dots under 1 h of continuous illumination.

a broad UV-Vis absorption spectrum in the range of 250–600 nm and the strong absorption peak was centered at 375 nm.

The IFE between C-dots and MnO_2 nanosheets

C-dots–MnO_2 nanosheets mixture were prepared in C-dots colloid solution through the reduction of $KMnO_4$ with MES. The fluorescence of C-dots was quenched in the presence of MnO_2 nanosheets (Fig. S3†). The absorption spectrum of MnO_2 nanosheets (Fig. S2b†) was well overlapped with the excitation and emission spectrum of C-dots (Fig. 1c), which suggests that the fluorescence quenching may be caused by FRET or IFE. Considering that IFE does not change the fluorescence lifetime and FRET can shorten the fluorescence lifetime, the fluorescence lifetimes of C-dots, C-dots–MnO_2 nanosheets mixture were further measured respectively. As shown in Fig. 2a and Table S1,† the fluorescence lifetime of C-dots was 5.80 ns. After mixing with MnO_2 nanosheets, the fluorescence lifetime of C-dots was 5.71 ns. The UV-Vis absorption spectra of MnO_2 nanosheets in the absence and presence of C-dots kept unchanged (Fig. 2b), indicating that no new substances were formed in the process of mixing. The nearly unchanged lifetime and absorption peaks indicated that the quenching of fluorescence was mainly caused by IFE, not FRET. The TEM image and HRTEM image of C-dots–MnO_2 nanosheets mixture was also measured, as shown in Fig. 2c and d, C-dots were deposited on the surface of MnO_2 nanosheets. However, because of the electrostatic repulsion between C-dots and MnO_2 nanosheets (Fig. S4†), no new composites were formed and the distance between them was not close enough to trigger FRET.

Interaction between GSH and MnO_2 nanosheets

When GSH was added to C-dots–MnO_2 nanosheets, MnO_2 could be reduced to Mn^{2+} by GSH, and meanwhile itself was oxidized to glutathione disulfide (GS–SG), thus the IFE process was destroyed and the fluorescence of C-dots was recovered (Fig. S3†). While when GSH were added to C-dots directly, the fluorescence intensity of C-dots kept almost unchanged, indicating GSH had no effect on the fluorescence of C-dots, and the fluorescence recovery of C-dots was mainly attributed to the reduction of MnO_2 nanosheets. To verify this, the fluorescence lifetime of C-dots–MnO_2 nanosheets mixture reacted with GSH were further measured. As shown in Fig. 2a, after reacting with GSH, the fluorescence lifetime of C-dots came back to 5.77 ns, suggesting that IFE process was destroyed due to the reduction of MnO_2 nanosheets. The fluorescence quantum yield (QY) were also measured using quinoline sulfate (QY = 54% in 0.1 M H_2SO_4) as a reference dye. After mixing with MnO_2 nanosheets, the QY of C-dots decreased from 34.59% to 8.80%. When GSH was added to C-dots–MnO_2 nanosheets mixture, the QY of C-dots reached 31.52% accordingly. As depicted in Fig. S5,† the

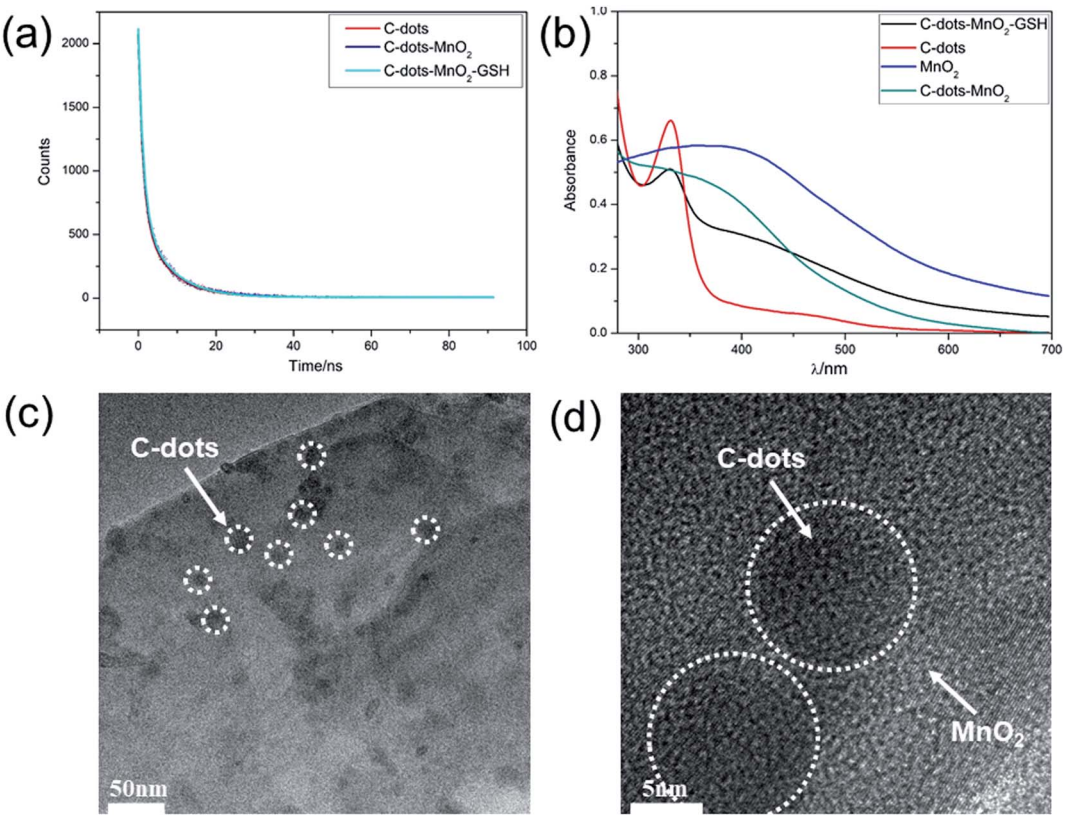

Fig. 2 (a) Fluorescence lifetime of C-dots, C-dots–MnO_2 nanosheets mixture, and C-dots–MnO_2 nanosheets mixture reacted with GSH. (b) The UV-Vis absorption spectra of C-dots, MnO_2 nanosheets, C-dots–MnO_2 nanosheets mixture, and C-dots–MnO_2 nanosheets mixture reacted with GSH. (c) TEM image of C-dots–MnO_2 nanosheets mixture. (d) HRTEM image of C-dots-MnO_2 nanosheets mixture.

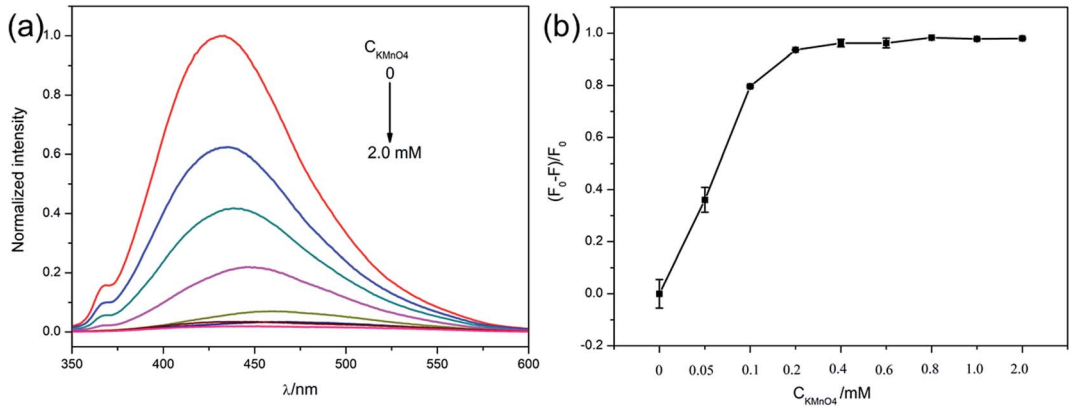

Fig. 3 (a) Fluorescence spectra of C-dots (0.035 mg mL^{-1}) in the presence of different concentrations of $KMnO_4$ (0, 0.05, 0.1, 0.2, 0.4, 0.6, 0.8, 1.0, 2.0 mM). (b) The plot of fluorescence quenching efficiency against the concentration of MnO_2 nanosheets.

XPS of MnO_2 nanosheets presents two peaks located at 641.1 and 653.4 ev, corresponding to Mn $2p_{3/2}$ and Mn $2p_{1/2}$ of MnO_2, respectively. In the presence of GSH, the intensity of the two peaks decreased significantly, indicating that MnO_2 nanosheets were transformed to Mn^{2+}.

Optimization of experimental conditions

To achieve the best sensing performance, the concentration of the MnO_2 nanosheets were first optimized, which was achieved by adjusting the amount of $KMnO_4$. As shown in Fig. 3a, the fluorescence intensity of C-dots was gradually quenched with the increase of $KMnO_4$. The maximum fluorescence quenching efficiency (96.21%) was observed when the concentration of $KMnO_4$ reached 0.4 mM. When $KMnO_4$ concentration kept on increasing, the quenching efficiency reached a relative stability state (Fig. 3b). Therefore, 0.4 mM of $KMnO_4$ were chosen as the optimal amount and used in the following study.

Before applying the system to GSH detection, the fluorescence recovery on the basis of time was first measured to monitor the kinetics of the reaction between C-dots–MnO_2 mixture and GSH. As shown in Fig. S6a,† with the extension of reaction time, the fluorescence signal of C-dots increased gradually and reached a stable stage after reacting for 20 min. So 20 min was selected as the optimal reaction time between C-dots–MnO_2 mixture and GSH. As can be seen in Fig. S6b,† after reacting with GSH, MnO_2 nanosheets were destructed, result in the release of C-dots and the recovery of fluorescence.

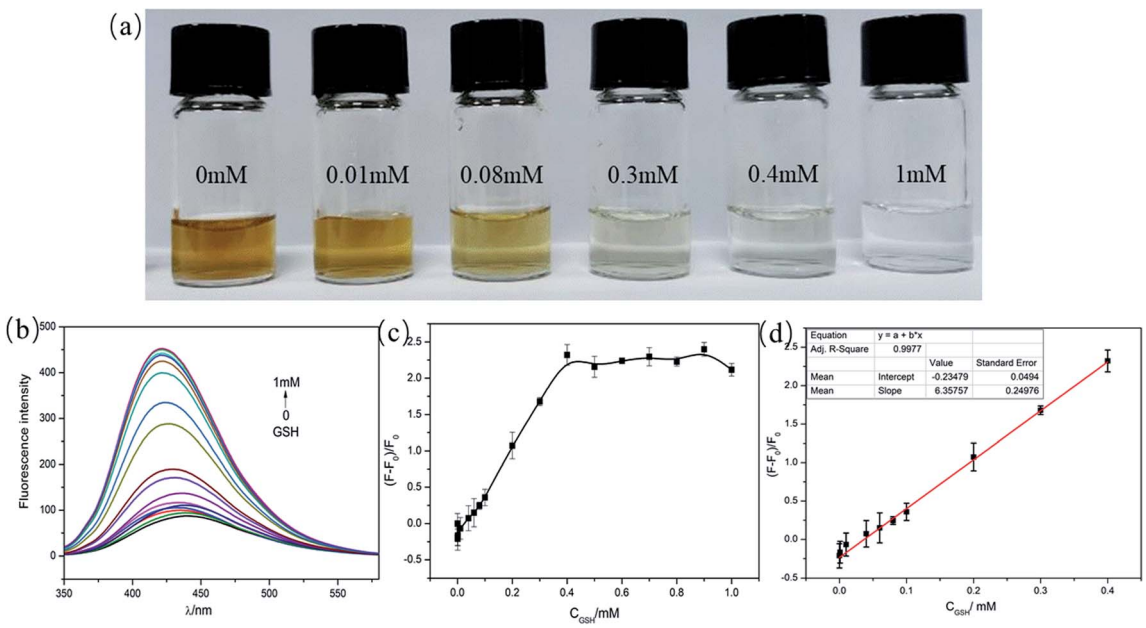

Fig. 4 (a) The photoshop of C-dots–MnO_2 mixture with various concentrations of GSH (0, 0.01, 0.08, 0.3, 0.4, 1.0 mM). (b) Fluorescence spectra of the C-dots–MnO_2 mixture in the presence of different concentrations of GSH (0, 0.1, 1, 10, 40, 60, 80 μm and 0.1, 0.2, 0.3, 0.4, 0.5, 0.6, 0.7, 0.8, 0.9, 1.0 mM). (c) The relationship between the fluorescence recovery and the concentration of GSH. (d) The linear plot of fluorescence recovery *versus* the concentration of GSH.

Table 1 Comparison of this work with earlier reported fluorescent probes for the detection of GSH

Probes	Strategy	Detection mode	Linear range	LOD	Ref.
UCNPs–MnO_2	FRET	Fluorescence	Not given	0.9 μM	13
PLNPs–MnO_2	FRET	Fluorescence	0–100 μM	0.83 μM	14
g-C_3N_4–MnO_2	FRET	Fluorescence	Not given	0.2 μM	15
Carbon dots–MnO_2	FRET	Fluorescence	0.2–600 μM	22 nM	33
QDs–MnO_2	FRET	Fluorescence	0.010–0.48 mM	0.61 μM	11
CuNCs–MnO_2	FRET	Fluorescence	0–300 μM	100 nM	18
PDA nanoparticles–MnO_2	Not mentioned	Fluorescence	0–350 μM	1.5 μM	39
BNQDs–MnO_2	IFE	Fluorescence	0.5–250 μM	150 nM	27
C-Dots–MnO_2	IFE	Colorimetry/fluorescence	0.1–400 μM	6.6 nM	This work

Colorimetric and fluorescence dual-readout assay of GSH in buffer

This assay was then applied to detected different concentrations of GSH by colorimetric and fluorescence dual-readout mode. As shown in Fig. S7,† the absorbance of C-dots–MnO_2 nanosheets mixture decreased gradually with the increase of GSH concentration from 0 to 1 mM. The color of solutions changed from brownish yellow to transparent gradually (Fig. 4a). The qualitative limit of GSH could reach 10 μM with naked eye. Considering the GSH content in biological samples (mM level), this method can realize the naked eye qualitative judgment of GSH content in actual samples. Simultaneously, the fluorescence of C-dots restored gradually (Fig. 4b) and reached a maximum at the concentration of 1 mM (Fig. 4c). A linear relationship between the fluorescence recovery and the concentration of GSH was found within the range from 0.1–400 μM, with a R^2 of 0.9977 (Fig. 4d). The limit of detection (LOD) of this system was calculated to be as low as 6.6 nM. Compared to the previous reported fluorescent probes for GSH detection (Table 1), the detection range and sensitivity of our system was significantly improved, which get benefit from the superior light absorption capability of MnO_2 nanosheets and the well spectral overlap between MnO_2 nanosheets and C-dots. In our IFE-based system, the distance between fluorophore and absorber was not strictly required, making the assembly mode between them more flexible. More importantly, the colorimetric and fluorescence dual-readout mode could realize qualitative and quantitative detection of GSH at the same time without additional equipments.

Specificity, reproducibility and stability for GSH

For further investigating the specificity of this C-dots–MnO_2 composites system, different kinds of substances including metal ions, amino acids, and other biomolecules (such as glucose and uric acid) were added to C-dots–MnO_2 nanosheets system to investigate the change of fluorescence intensity. As shown in Fig. 5, the fluorescence recovery in the presence of GSH (0.4 mM) was significantly higher than that of other substances (0.2 mM for uric acid, and 0.4 mM for others), in which the concentration of uric acid was determined according to its concent in normal human urine.[40,41] It is noteworthy that other reducing agents in biological samples such as cysteine (Cys), homocysteine, and ascorbic acid (AA) could also induce fluorescence recovery by reducing MnO_2 nanosheets to Mn^{2+}. But the interferences of these distractors in biological samples are usually ignored because the concentrations of distractors were obviously lower than that of GSH.[42] So this system showed considerable selectivity towards GSH in blood, urine and other biological samples.

Then intra-assay and inter-assay precision were used to investigate the reproducibility of this biosensor. The C-dots–MnO_2 nanosheets mixture prepared on the same and different batches were used to detect GSH with the same concentration (0.4 mM). The results showed that their RSDs of five parallel detections were less than 4% for the same batch C-dots–MnO_2 nanosheets mixture, and less than 8% for different batch, indicating the acceptable reproducibility of this C-dots–MnO_2 nanosheets system. To investigate the stability of this biosensor, the inter-day and intra-day precision were measured. As shown in Fig. S8a,† C-dots–MnO_2 nanosheets mixture were used to detect GSH (0.4 mM) every two hours on the same day, the change degree of response signal was less than 3%. After been storage at 4 °C for 14 days, the change degree of response signal was less than 5% (Fig. S8b†), indicating that the

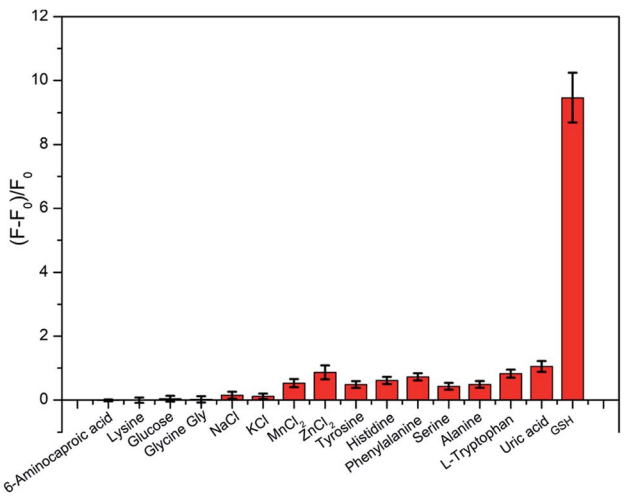

Fig. 5 The fluorescence recovery of C-dots–MnO_2 mixture with 0.4 mM of GSH and different kind of interferences (0.2 mM for uric acid, and 0.4 mM for others).

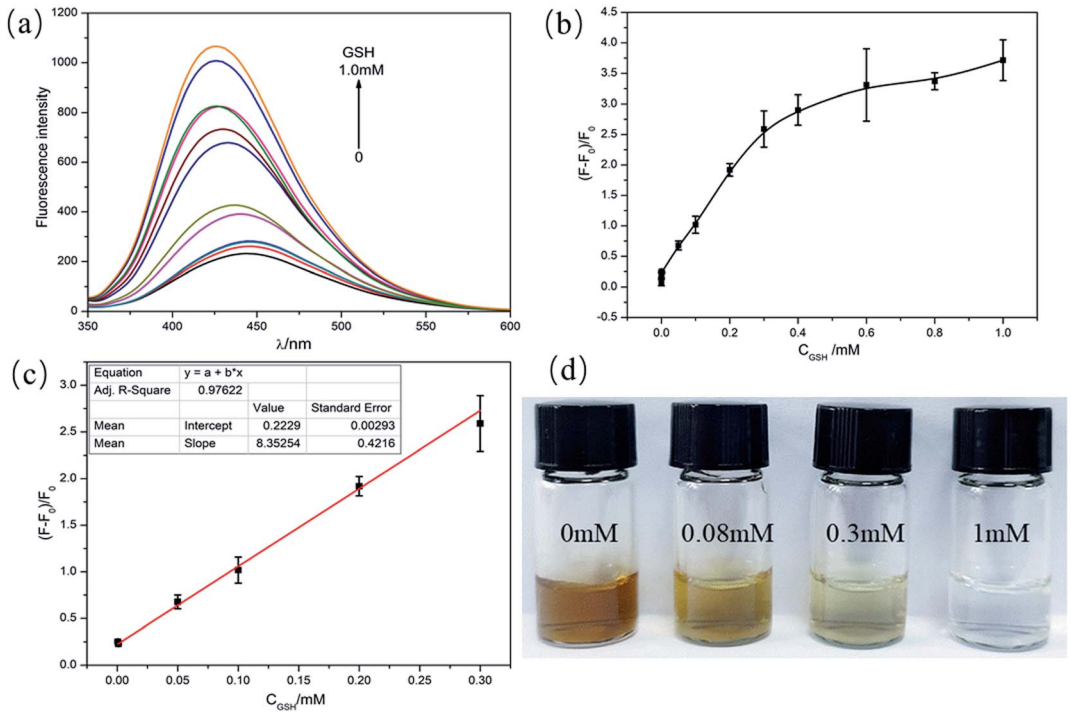

Fig. 6 (a) Fluorescence spectra of C-dots–MnO_2 mixture with various concentrations of GSH (0–1.0 mM) in 400-fold diluted human serum. (b) The dependence of fluorescence recovery and GSH concentration. (c) Calibration plot of fluorescence recovery *versus* GSH concentration. (d) The photoshop of C-dots–MnO_2 mixture with different concentrations of GSH (0, 0.08, 0.3, 1.0 mM) in 400-fold diluted human serum.

biosensor exhibited satisfactory stability during manufacture, normal storage, long-distance transport.

Detection of GSH in human serum and urine

To validate the feasibility of this method in complex biological samples, determination of GSH in human serum and urine were further explored. Considering the concentration of GSH in biological samples and the detection range of our strategy, human serum and urine samples were diluted with buffer before been used as analysis medium. As shown in Fig. 6 and S9,† the fluorescence of carbon dots gradually recovered with the increase of GSH concentration, which was similar to that in buffer. The fluorescence recovery was proportional to GSH concentration with a linear range of 0.5–300 μM (Fig. 6c and S9c†). The LOD in human serum and urine sample were 15 nM and 6.9 nM, respectively. More interestingly, the concentration of GSH in biological samples could also be distinguished by naked eye. When GSH concentration reached 0.08 mM, the color of the C-dots–MnO_2 composites became lighter, indicating that GSH at this concentration can be distinguished by naked eyes (Fig. 6d and S9d†). With the further increase of GSH concentration, the color of the solution gradually faded and became clear and transparent when the concentration of GSH reached 1.0 mM.

Conclusions

In summary, an ultrasensitive colorimetric and fluorescence dual-readout assay based on carbon dots–MnO_2 mixture was established for the determination of GSH. This sensing system could not only realize the quantitative detection of GSH, but also qualitatively determine the concentration of GSH through naked eyes. Meanwhile, this assay exhibit satisfactory responses toward GSH in human serum and urine samples. It indicates that this strategy has a great potential for GSH-related disease diagnosis and biological application.

Ethics statement

Serum samples were collected from Hospital of Xinyang Normal University. All experiments were performed and followed incompliance with the guidelines of clinical sample management rules of Hospital of Xinyang Normal University, and approved by the Ethics Committee at Xinyang Normal University. Informed consents were obtained from human participants of this study.

Conflicts of interest

There are no conflicts to declare.

Acknowledgements

This work was supported by the National Natural Science Foundation of China (No. 21804117), the Key Scientific and Technological Project of Henan Province (182102310703), and the Nanhu Scholars Program for Young Scholars of XYNU.

Notes and references

1 C. L. Shelly, *FASEB J.*, 1999, **13**, 1169–1183.
2 R. L. Krauth-Siegel, H. Bauer and R. H. Schirmer, *Angew. Chem., Int. Ed.*, 2005, **44**, 690–715.
3 C. Peng, H. Xing, X. Fan, Y. Xue, J. Li and E. Wang, *Anal. Chem.*, 2019, **91**, 5762–5767.
4 J. C. Harfield, C. Batchelor-McAuley and R. G. Compton, *Analyst*, 2012, **137**, 2285–2296.
5 Y. Wang, J. Lu, L. H. Tang, H. X. Chang and J. H. Li, *Anal. Chem.*, 2009, **81**, 9710–9715.
6 J. Tang, B. Kong, Y. Wang, M. Xu, Y. Wang, H. Wu and G. Zheng, *Nano Lett.*, 2013, **13**, 5350–5354.
7 J. Yu, C. Li, S. Shen, X. Liu, Y. Peng and J. Zheng, *Rapid Commun. Mass Spectrom.*, 2015, **29**, 681–689.
8 N. K. Wawegama, G. F. Browning, A. Kanci, M. S. Marenda and P. F. Markham, *Clin. Vaccine Immunol.*, 2014, **21**, 196–202.
9 A. Saha and N. R. Jana, *Anal. Chem.*, 2013, **85**, 9221–9228.
10 X. F. Yang, Q. Huang, Y. Zhong, Z. Li, H. Li, M. Lowry, J. O. Escobedo and R. M. Strongin, *Chem. Sci.*, 2014, **5**, 2177–2183.
11 Y. Y. Mi, X. X. Lei, H. Y. Han, J. G. Liang and L. Z. Liu, *Anal. Methods*, 2018, **10**, 4170–4177.
12 Q. Wang, L. Li, X. Wang, C. Dong and S. Shuang, *Talanta*, 2020, **219**, 121180.
13 R. Deng, X. Xie, M. Vendrell, Y. T. Chang and X. Liu, *J. Am. Chem. Soc.*, 2011, **133**, 20168–20171.
14 N. Li, W. Diao, Y. Han, W. Pan, T. Zhang and B. Tang, *Chemistry*, 2014, **20**, 16488–16491.
15 X. L. Zhang, C. Zheng, S. S. Guo, J. Li, H. H. Yang and G. Chen, *Anal. Chem.*, 2014, **86**, 3426–3434.
16 A. Garcia-Marin, J. M. Abad, E. Ruiz, E. Lorenzo, J. Piqueras and J. L. Pau, *Anal. Chem.*, 2014, **86**, 4969–4976.
17 L. M. Shen, Q. Chen, Z. Y. Sun, X. W. Chen and J. H. Wang, *Anal. Chem.*, 2014, **86**, 5002–5008.
18 H.-B. Wang, Y. Chen, Y. Li and Y.-M. Liu, *RSC Adv.*, 2016, **6**, 79526–79532.
19 P. G. Luo, S. Sahu, S. T. Yang, S. K. Sonkar, J. Wang, H. Wang, G. E. LeCroy, L. Cao and Y. P. Sun, *J. Mater. Chem. B*, 2013, **1**, 2116–2127.
20 X. Shi, W. Wei, Z. Fu, W. Gao, C. Zhang, Q. Zhao, F. Deng and X. Lu, *Talanta*, 2019, **194**, 809–821.
21 F. Qu, H. Pei, R. Kong, S. Zhu and L. Xia, *Talanta*, 2017, **165**, 136–142.
22 C. Y. Ji, Y. Q. Zhou, R. M. Leblanc and Z. L. Peng, *ACS Sens.*, 2020, **5**, 2724–2741.
23 M. Y. He, N. Shang, L. Shen and Z. H. Liu, *Analyst*, 2020, **145**, 4181–4187.
24 M. Y. He, N. Shang, Q. R. Zhu and J. Xu, *Anal. Chim. Acta*, 2021, **1143**, 93–100.
25 Y. Hu, L. Zhang, X. Geng, J. Ge, H. Liu and Z. Li, *Anal. Methods*, 2017, **9**, 5653–5658.
26 J. Yang, Z. Huang, Y. Hu, J. Ge, J. Li and Z. Li, *New J. Chem.*, 2018, **42**, 15121–15126.
27 X. Tan, P. Zhang, C. Ye, Y. Min, Q. Li and Y. Wang, *Dyes Pigm.*, 2020, **180**, 108515.
28 L. Xue, F. Huang, L. Hao, G. Cai, L. Zheng, Y. Li and J. Lin, *Food Chem.*, 2020, **322**, 126719.
29 B. Dong, H. Li, J. Sun, G. M. Mari, X. Yu, Y. Ke, J. Li, Z. Wang, W. Yu, K. Wen and J. Shen, *Sens. Actuators, B*, 2019, **286**, 214–221.
30 Y. Lin, Q. Zhou, D. Tang, R. Niessner and D. Knopp, *Anal. Chem.*, 2017, **89**, 5637–5645.
31 C. Yang, W. Deng, H. Liu, S. Ge and M. Yan, *Sens. Actuators, B*, 2015, **216**, 286–292.
32 Y. Wang, K. Jiang, J. Zhu, L. Zhang and H. Lin, *Chem. Commun.*, 2015, **51**, 12748–12751.
33 Q. Y. Cai, J. Li, J. Ge, L. Zhang, Y. L. Hu, Z. H. Li and L. B. Qu, *Biosens. Bioelectron.*, 2015, **72**, 31–36.
34 N. Sohal, B. Maity and S. Basu, *ACS Appl. Nano Mater.*, 2020, **3**, 5955–5964.
35 X. Tan, P. Zhang, C. Y. Ye, Y. H. Min, Q. W. Li and Y. Wang, *Dyes Pigm.*, 2020, **180**, 108515.
36 X. W. Mu, M. X. Wu, B. Zhang, X. Liu, S. M. Xu, Y. B. Huang, X. H. Wang, D. Q. Song, P. Y. Ma and Y. Sun, *Talanta*, 2021, **221**, 121463.
37 X. Y. Sun, M. J. Yuan, B. Liu and J. S. Shen, *RSC Adv.*, 2018, **8**, 19786–19790.
38 T. Z. Li, Y. T. Gao, H. Y. Li, C. Y. Zhang, Y. F. Xing, M. Jiao, Y.-E. Shi, W. Li, Y. Q. Zhai and Z. G. Wang, *Analyst*, 2020, **145**, 5206–5212.
39 X. J. Kong, S. Wu, T. T. Chen, R. Q. Yu and X. Chu, *Nanoscale*, 2016, **8**, 15604–15610.
40 A. Pastore, R. Massoud, C. Motti and G. Federici, *Clin. Chem.*, 1998, **44**, 825–832.
41 Y. Y. Liu, H. C. Li, B. Guo, L. J. Wei, B. Chen and Y. Y. Zhang, *Biosens. Bioelectron.*, 2017, **91**, 734–740.
42 R. Deicher, F. Ziai, C. Bieglmayer, M. Schillinger and W. H. Horl, *J. Am. Soc. Nephrol.*, 2005, **16**, 1811–1818.